Fast Processes in a N 2 O–Modulated Hollow Cathode Discharge: Excitation and Diffusion

ARTICLE *in* THE JOURNAL OF PHYSICAL CHEMISTRY A · SEPTEMBER 2000

Impact Factor: 2.69 · DOI: 10.1021/jp0010177

FAST PROCESSES IN A N_2O MODULATED HOLLOW CATHODE DISCHARGE: EXCITATION AND DIFFUSION

T. de los Arcos, M. Castillo, C. Domingo, V. J. Herrero, M. M. Sanz[♣], and I. Tanarro*

Instituto de Estructura de la Materia (CSIC), Serrano 123, 28006 Madrid, Spain

[♣]Departamento de Física Aplicada, Universidad Alfonso X el Sabio, Villanueva de la Cañada, 28691 Madrid, Spain

*Corresponding author. Fax: +34.91.5855184; e-mail: itanarro@iem.cfmac.csic.es

Abstract

In this work the changes in the infrared absorption of N_2O observed in a hollow cathode discharge modulated by a 45 Hz square wave are studied by time resolved infrared absorption spectroscopy, with a Fourier transform infrared (FTIR) spectrometer working in the step-scan mode. These variations are attributed to alternative population and depopulation of the ground state of N_2O; on the other hand, no changes are observed in the total concentration of N_2O and the major products of the discharge. The experimental results are explained by means of a simple kinetic model: vibrational excitation processes are assumed to be the main cause of the observed effects, but an inhomogeneous distribution of the stable species and the incorporation of diffusion terms between the plasma volume and the rest of the discharge cell are shown to be crucial in order to justify the quick and sharp variations in the N_2O ground state population seen along the path of the IR beam. The influence of these effects has been verified also by mass spectrometric measurements of the temporal behavior of the concentration of the major products N_2O, N_2 and O_2 at one end of the discharge cell and at different frequencies.

1. Introduction

The cold plasmas occurring in glow discharges are non equilibrium systems characterized by a comparatively hot (several eV on average) electron energy distribution and much colder (close to room temperature) energy distributions for the heavier neutrals**.** Electronic collisions within these plasmas unleash a series of processes giving rise to a rich physico-chemistry with practical applications in many fields and most notably in the processes of deposition of chemical vapors and surface conditioning. Plasma enhanced chemical vapor deposition (PECVD) and plasma assisted surface modification are nowadays well established technological tools[1] offering an advantageous alternative to the higher temperature thermal procedures. Till now, PECVD has been used mainly with RF and MW discharges, but recently, an increasing growth in papers reporting DC or low frequency plasmas for PECVD is found[2-5], since particle formation can be largely avoided, even with room-temperature substrates,[2] on the other hand, with DC plasmas, larger surfaces can be coated in a simpler way, as needed for example in the conditioning of nuclear fusion vessels[6] and in the cleaning and hardening[1] of large surfaces. In that cases, diffusion effects may be critical in determining the homogeneous distribution of the films, depending on the geometry of the discharge and, specially, when the input of the precursor is localized at a single point and high dissociation rates are present.

The undeniable practical advantages of cold plasmas are not paralleled by a corresponding ease for the analysis of the mechanisms ultimately responsible for their properties. The complex kinetics taking place in them, which includes electron impact dissociation, ionization and excitation, non reactive quenching, gas phase homogeneous chemistry, heterogeneous wall reactions, diffusion etc., is extremely difficult to unravel. As a result, the progress in the applications of these plasmas is largely empirical. A theoretical modeling of these systems providing a clear insight into the atomic and molecular mechanisms, though highly desirable, is usually far from satisfactory. Due to the scarcity of data on cross sections and rate constants, either from experiment or theory, for many of the relevant elementary processes, plasma models are often plagued with daring hypothesis and dubious assumptions. As a rule, a thorough experimental diagnostics is the only way to make sound advances in the modeling.

Nitrous oxide is often used, together with different silicon compounds, in the PECVD of SiO_2 oxide and thus, its glow discharges have deserved some attention and reliable information about its kinetics is already available. Former studies have concentrated on the diagnosis and modeling of steady state glow discharges of N_2O and of its mixtures with inert gases.[7-12] In a previous work,[12] we extended the studies of Cleland and Hess[7] and of Kline et al.[8] on rf discharges of pure N_2O by using a DC hollow cathode discharge and combining various analytic tools (namely double Langmuir

probes, Fourier-Transform infrared spectroscopy and mass spectrometry) for the diagnosis of the steady state plasma. Our data could be essentially described with a relatively simple set of kinetic equations based on the former models of refs 7, 8 except for the appearance of NO_2 , a minor but clearly identifiable component of our plasma that was not detected in the previous rf works. In order to justify the presence of NO_2 we had to introduce in the model an heterogeneous reaction at the steel walls of the cathode.

Plasma modeling is not only hampered by the lack of reliable data about many of the relevant elementary processes, but also by the difficulties for an experimental observation of many of the species involved, specially the most reactive and unstable ones. However, even restricting the observations to a reduced set of species, one can still take advantage of the hierarchy of characteristic dynamical times involved in the global kinetics of the discharge and perform measurements with different time resolution. A suitable way of doing it is the use of modulated discharges of different frequencies.

In a recent work[13] we analyzed the transients associated with the ignition and extinction of the discharge with a time resolution in the order of the second and disclosed the role of new electron impact dissociation processes that were not apparent in the steady state measurements; besides, previous assumption of an heterogeneous wall reaction as the main source of the observed NO_2 was not born out by the time resolved measurements and a reaction of vibrationally excited nitrous oxide was invoked. The significant presence of N_2O (001) in the plasma was demonstrated by emission spectroscopy, but the process of electron impact vibrational excitation of N_2O, assumed to be the origin of the N_2O (001) found in the plasma, is too fast[14] to be directly detectable with the time resolution of this experiment.

In order to evince in a more clear way the role of the faster processes, we present in this study the diagnosis and modeling of a 45 Hz modulated hollow cathode discharge with a time resolution of the order of a millisecond, appropriate for the investigation of the effects of diffusion and electron impact excitation under our experimental conditions. These phenomena are so fast for populating and depopulating the ground state of species such as N_2O, that their effects in the stationary state of a continuous discharge or during the transients of a very low frequency modulated one, can go unnoticed in comparison with the remarkably slower but larger changes originated by dissociation, ionization, homogenous or heterogeneous processes. The experimental upgrading needed for these faster measurements is described and the validity and limitations of the previous kinetic model[13] is checked against the new data.

2. Experimental measurements

The experimental measurements carried out in the present work were obtained with a hollow cathode discharge cell specially designed for both absorption and emission spectroscopy, and mass spectrometry. Time resolved absorption measurements were taken by means of a Fourier Transform Infrared Spectrometer (FTIR) Bruker IFS66, used in the step-scan mode. Charge density and mean electron energy were measured with a double Langmuir probe built in our laboratory. Besides, a quadrupole mass spectrometer Balzers QMG112 was employed to study the temporal behavior of the concentration of the major products of the N_2O discharge.

A scheme of the hollow cathode discharge cell is shown in Figure 1; it is just the same one used in references.[12,13,15] In Figure 1, the focusing and the optical path of the IR beam of the spectrometer across the cell are indicated, the length of the cell is the maximum one compatible with the dimensions of the absorption sample chamber of the FTIR spectrometer. For time resolved absorption spectroscopy measurements, the discharge was modulated with a 45 Hz square wave electrical signal and a current of 80 mA. This frequency was selected in such a way that it was low enough to allow an efficient modulation of the IR absorption signal due to the N_2O excitation and relaxation processes to be studied here, but high enough to distinguish these processes from the slower but more intense ones studied in the previous work.[13] The measurements were taken at a 2 mbar pressure with two different gas flow rates of pure N_2O (99.5%): 3 sccm and 108 sccm, coincident with those employed in the previous paper. The cell was refrigerated by a continuous flow of water. A time interval of some 10 s was let between the ignition of the modulated discharge and the beginning of the acquisition process, in order to avoid the interference of the slow transients happening during this time until the attainment of the “stationary” state, which were studied in detail in Ref. 13.

The concentrations of the major stable species involved in the discharge, N_2O, N_2 and O_2, were studied with the mass spectrometer at different modulation frequencies, and no modulation at all was observed above 20 Hz for any of these species. Their steady state concentrations, as well as their evolution during the turning on and off of a DC discharge, were studied in detail in Refs.12 and 13 for various physical conditions. Extraction of the gas sample was performed at the center of one end of the cell through a holder with a 100 μm diaphragm, located in place of one of the IR windows, in the same way as in refs 12,13. The time constant of the mass spectrometric system was determined by the gas residence time in the quadrupole vacuum chamber, which was 12 ms, since the temporal response of the electronics was considerably smaller (2 ms with the amplification factor employed in this work).

The dependence of charge density and mean electron energy on longitudinal and radial position along the discharge cell were measured with a double Langmuir probe and a digital oscilloscope with special probes isolated from ground, in a similar way to that used in refs 12,15, with the discharge operating in the DC mode. In order to verify the speed with which the charge density is established or disappears following the square wave modulation of the discharge, the temporal response in electrical current of the Langmuir probe was collected for a constant value of the floating potential applied between the two wires. Once the discharge was turned on or off, the current intensity reached a constant value or disappeared respectively in less than 10 μs. This is in good agreement with other estimates found in the literature[16] and indicates that for the time scales of the present work the appearance of ions and electrons may be assumed to be instantaneous.

In a previous paper devoted to the study of the ignition and extinction slow processes of the discharge,[13] a single cycle of modulation lasting for several seconds was recorded for each whole measurement, and temporal resolution during this cycle was achieved with the FTIR spectrometer working in the continuous scan mode, in such a way that each interferogram was acquired completely before the next one, some 100 ms later. This temporal resolution is not sufficient at all to study by FTIR spectroscopy the transients corresponding to a 45 Hz discharge, so the interleaving-sampling technique based on the continuous-scan mode of operation or, alternatively, the step-scan technique (without phase modulation), can be selected to be used with this instrument under the present conditions. Both techniques are described in detail elsewhere.[17-19] Although the final data arrays produced by each option are similar, the differences in the methods imply substantial differences in the kind of measurements for which the two techniques are suited, and also in the potential noise sources to which they are subject. Basically, for short transients, which can be repeated at high rates, the interleaving methods are preferable, since step-scan techniques lead usually to more noisy spectra.[19] The main advantages of the step-scan technique are found in measurements where the maximum repetition rate of the experiment is relatively low (e.g. less than 100 Hz), because in the continuous-scan version there is a maximum time between initiations of the transients, imposed by the fact that the mirror has a minimum velocity, below which its movement becomes unstable.[20]

In the step-scan technique, the interferometer mirror is held at a fixed position during the time course of the process while the transient is digitized. In this way, by moving the mirror step-wise, one obtains the time courses of the change of the interferogram at each sampling point, and from the data set, the spectral changes can be obtained by performing the Fourier transform at each time of interest.

As far as we know, since the pioneering works of Murphy *et al.*[21,22] describing the step-scan time-resolved Fourier Transform spectroscopic method, this technique has been used for very few absorption measurements.[23,24] In contrast, a lot of references about time-resolved emission measurements can be found in the literature employing step-scan FTIR spectroscopy (see for example refs 17-19,21,22,25). This lack of absorption measurements is probably due to the difficulty associated with the huge difference, of some orders of magnitude, between the large intensity of the continuous infrared source (a Globar in our case), specially near the maximum of the interferogram, and the small amplitude of the modulated absorption signal. Small mechanical vibrations of the optical bench of the FTIR instrument, produce undesired displacements of the moving mirror; if these mirror shifts happen when it is located near the maximum of interference, they can cause oscillations in the amplitude of the signal (identified as noise) much larger than the amplitude of the true modulated absorption signal, even if the displacement is only of a few nanometers. Besides, time-resolved Fourier Transform Spectroscopic techniques require in general a much wider bandwidth than the non-time-resolved procedure, because the transients to be measured have usually high-frequency components, and this eliminates one of the great advantages associated with FTS: the ability to convert a wide range of optical frequencies into a relatively narrow band of lower frequencies and achieve noise rejection by the application of narrow band-pass electronic filters.[26] Furthermore, in the case of step-scan techniques and when no phase modulation is employed[27] this band of frequencies is located at the lowest end of the spectra, where electrical noise is highest.

In the present case, the hollow cathode discharge cell was installed in the sample compartment of the FTIR instrument, and the joints between the cell and the spectrometer were sealed with an elastomer material that prevented the entrance of wet air inside the interferometer. In order to reduce as much as possible the noise in the interferograms, it was necessary to isolate carefully the mechanical vibrations transmitted to the cell through the vacuum tubes coming from the rotary pump, and any other kind of mechanical instability. The IR detector employed in the present work was an MCT (HgCdTe), whose typical time constant is of the order of 1 ns. Its preamplifier was coupled in the DC mode. The cut-off frequency of the preamplifier was above 20 MHz. In order to increase the signal/noise ratio, each measurement, which covered a time interval of two discharge modulation periods, was averaged 32 times (i.e. ~1.4 s) with the mirror held at a constant position. Globally, a total duration of some 25 minutes was necessary to perform a whole set of time resolved single-sided interferograms with a spectral resolution of 40 cm^{-1} (932 data points, with the origin of the scan slightly advanced in relation with the maximum of the interferogram for phase adjust purposes). Before acquiring the interferograms of the modulated discharge, the reference

interferogram needed to transform transmittance spectra into absorbance spectra was taken with the empty cell. In spite of the averaging procedure, the signal/noise ratios reached in the present measurements are notably worse than those obtained with the rapid scan technique for the continuous or the low frequency modulated discharge. As a consequence, only the ν_1 and ν_3 bands of the N_2O could be obtained with sensitivity enough to characterize the temporal evolution of the ground state of N_2O; the temporal behavior of NO and NO_2 could not be studied at this modulation frequency. In order to obtain absolute concentrations of N_2O, the absorbance of the ν_3 band at a spectral resolution of 40 cm^{-1} was calibrated at different N_2O pressures. A slight widening of the bands was observed for the case of the highest N_2O flow rate during the discharge, thus, absolute concentration measurements performed with the N_2O discharge operating at 3 sccm flow rate are more reliable and precise than those performed at 108 sccm. Figure 2 a shows some of the time resolved absorbance spectra of the ν_3 band of N_2O used for these measurements, with a spectral resolution of 40 cm^{-1}. A series of ~ 40 spectra was recorded during each modulation cycle (sampling time: 0.55 ms). For clarity, only two of these spectra (with discharge “on” and “off”) are displayed for each of the two gas flow rates (3 and 108 sccm). Integration of the band was performed between 2100 and 2300 cm^{-1} in order to obtain the concentration. A Blackman-Harris function of 3 terms was used for apodization and phase correction was of the Mertz type. In order to compare, Figure 2 b shows a 2 cm^{-1} spectrum of a DC, 40 mA, 3 sccm, N_2O discharge between 1500 and 2700 cm^{-1}, obtained with the FTIR spectrometer working in the rapid scan mode; in this figure, the weak NO and NO_2 bands, as well as the 2 ν_1 and $\nu_1+2\nu_2$ N_2O bands can be observed too.

In Figure 3 the temporal evolutions of the ground state N_2O concentration experimentally obtained with the hollow cathode discharge operating at 45 Hz and 2 mbar are shown at the two gas flow rates, 3 sccm and 108 sccm, as well as the excitation signal. The data acquisition began in both cases once the ignition transient of the modulated discharge had finished and a pseudo-stationary state had been reached (i.e. ~ 10 - 20 s after the turning on of the plasma). As can be seen, very different values of the mean N_2O concentration in the ground state were obtained with each value of the gas flow rate. This difference is mainly due to the influence of the slow dissociation and chemical processes happening in the discharge;[13] in this sense the 45 Hz square wave modulated discharge could be considered on average like a DC discharge with half the current intensity. On the contrary, the modulated components of the signals reveal the existence of much faster processes and are very similar for both flow rates, with rise and decay responses approximately exponential, and characteristic times of the order of one or two milliseconds. In Figure 3, the simulation of the discharge with the model developed in ref 13 is also shown. As can be seen, the appearance of the

rapid and relatively large amplitude transients experimentally observed cannot be explained with that model. Improvements in the theoretical treatment of the modulated discharge are thus needed in order to obtain a better description of its behavior. Figure 3 also includes the results of the improved kinetic model used finally in the present work, which will be described in the next section.

3. Kinetic model

The kinetic model used here was firstly developed in an attempt to explain the processes involved in a DC hollow cathode N_2O discharge,[12] and was subsequently upgraded in order to predict also the slow transient effects, with characteristic times of some seconds, that could be observed experimentally during the ignition and the extinction of that discharge.[13] Nevertheless further improvements have been required in this work, in order to reproduce, at least qualitatively, the variations suffered by the ground state population of the precursor N_2O, with characteristic times of some milliseconds, that can be observed when the discharge is periodically modulated at higher frequencies. As explained briefly in the previous section, these transients cannot be attributed to the relatively slow dissociation processes by electronic impact, which initialize the whole chemistry of the discharge, or to chemical reactions, but are found to be attributable fundamentally to faster processes that do actually happen in the discharge too: the excitation of the N_2O ground state by electronic impact which was already included in the kinetic model, followed by quick de-excitation processes, and the very significant diffusion effects, which could be overlooked when considering slower transients, but are found to be crucial in the present case. Due to this fact, the former assumption that the stable species were homogeneously distributed along the whole cell volume can be no longer maintained.

The kinetic model has been kept as simple as possible, both in the number of chemical reactions and in the physical phenomena considered. The set of relevant differential equations has been numerically integrated, like in the former papers.[12,13] Diffusion effects have not been incorporated actually as a three-dimensional problem depending locally of each position; instead, two different volumes have been distinguished: the plasma volume, and the rest of the cell. In each of the two volumes the concentrations of the stable products may be different, but are assumed to be homogeneously distributed; in the kinetic model the two volumes are inter-communicated just by diffusion processes. Furthermore, an elementary geometry with cylindrical symmetry has been assumed and diffusion has been considered to take place effectively just along the direction of the symmetry axis of the cylinder.

In a previous paper,[12] the set of kinetic reactions considered in the modeling of the N_2O discharge was evaluated in detail; therefore, only a brief description of the individual processes taken into account in both cases will be given here, with a more extended explanation of the improvements needed to simulate suitably the 45 Hz modulated discharge.

Excitation processes. In the present model, vibrational excitation by electronic impact of the fundamental, the symmetric (100), and asymmetric (001) vibrational stretching modes of N_2O are found to be the main cause of the rapid variations of the N_2O ground state population observed in the modulated hollow cathode discharge. In the previous work[13] the rate constants for the vibrational excitation of these levels were already included in the global kinetics, but the effect of these fast processes could not be observed directly. These rate constants, remarkably large, are two orders of magnitude higher than the dissociation ones due to resonances in the excitation cross sections for electron energies close to the electron mean energy found in the present discharge[14] (see Table I).

Vibrational excitation to the bending mode (010) of N_2O has not been incorporated, since its cross section by electronic impact is ~ 50 times smaller than that of the (100) state[14] at the electron energies found in the N_2O hollow cathode discharge (measured mean value ~ 3 eV, assuming a Maxwellian distribution[15]). The excitation cross section of this (010) level increases by decreasing electron energy down to 0.1 eV, but it is in any case at least ten times smaller than that of the (100) stretching mode. Excitations by electronic impact to overtone vibrational modes or to excited electronic levels of N_2O have not been considered, since, to our knowledge, there is no information about these processes. Rotational excitation is efficient in collisions with low energy electrons but it has not been included either because the collisional relaxation of the N_2O rotation at the working pressure of 2 mbar is very fast [28] (<1 μs) in comparison with the vibrational one[13] (>1 ms for the (001) mode). In fact, an approximate Boltzman distribution of the rotational levels corresponding to the ambient temperature can be assumed, as it was shown experimentally in Figure 3 of ref 12, where the absorbance spectrum of N_2O during a 40 mA DC hollow cathode discharge displays a population distribution corresponding to a temperature lower than 325 K. In contrast, emission spectra of the same discharge showed vibrational temperatures of ~ 1300 K for the (001) asymmetric stretching mode. In any case, the inclusion of additional excitation terms of N_2O into the kinetic model would lead to an increase of the predicted amplitude of modulation of the N_2O ground state population with the modulated discharge, in better agreement with the present experimental results; the same effect would be obtained with excited levels of the other products of the discharge, provided they could couple efficiently with the N_2O excitation or with the physico-chemical mechanisms considered in the model.

Dissociation. Electron impact dissociation of N_2O is the key process in the chemical kinetics of the hollow cathode discharge and it is responsible of the partial disappearance of this species;[12,13] once the steady state has been reached, in a typical time scale of a few seconds. This long term depletion can be observed in Figure 3, where the value of the initial N_2O concentration, which can be assumed to correspond essentially to the ground vibrational state, is shown together with the value of the ground state N_2O population recorded with the FTIR spectrometer, once the steady state of the modulated discharges has been reached. Note specially the small value of the mean ground state N_2O concentration left in the discharge at the lower gas flow rate ($\sim 1.5 \times 10^{16}$ cm^{-3}) as compared to the initial value ($\sim 5.3 \times 10^{16}$ cm^{-3}). Nevertheless, the dissociation rate constants of N_2O, notably smaller than the excitation ones, combined with the low electron concentrations in the plasma, cannot justify the fast variations observed in the ground state N_2O concentration, which correspond to the modulation of the discharge. In this work, the same three N_2O electron dissociation channels assumed in ref 13 have been considered, each one with the same rate constants when applied to the ground state and to the (100) and (001) vibrationally excited N_2O levels (see Table I).

De-excitation. In the former works[12,13,15] it was seen that the most significant excited species involved in the chemical kinetics of the discharge was the $O(^1D)$, and consequently, the same de-excitation and reaction channels involving this species, with the same rate constant values, have been taken into account in the present work. Chemical reactions and quenching of the excited oxygen atoms have relatively large rate constants. Nevertheless, $O(^1D)$ elementary processes turn out to be too slow, as compared with the vibrational excitation and de-excitation of the nitrous oxide, to justify the experimental results studied here. In the present work, the same vibrational de-excitation processes involving the (100) and (001) levels of N_2O considered previously have been included: spontaneous emission, quenching with N_2O in its ground state, and diffusion outwards the plasma volume with possible de-excitation by collision on the wall; all of them with the same lifetimes or rate coefficients assumed previously. In general, they are relatively fast processes, which happen in time scales of milliseconds.

Homogeneous reactions. As it is shown in Table I, for the sake of coherence all the homogeneous reactions included in ref 13 have been considered in the present work.

Heterogeneous reactions. The set of heterogeneous reactions included in the current work and shown in Table I is also the same included in ref 13, although only wall deactivation of vibrationally excited N_2O, may be of significance. On the contrary, processes affecting mainly the concentrations of the minor products do not influence notoriously the changes in the populations of the N_2O ground state and its excited vibrational levels.

Differential Equations. As shown in Table II, the present kinetic model is based on the resolution of two sets of interdependent coupled differential equations, obtained from the reactions included in Table I. One of these sets accounts for the reactions and processes occurring in the plasma volume, V_P, initiated by the dissociation and electron impact excitation of the N_2O molecules in this volume, which are renewed partly due to gas flow input and partly by diffusion from the rest of the reactor. It is just in this plasma volume where the transient species are assumed to be confined and where the stable products are generated. The other set of differential equations explains what happens in the remaining volume of the reactor, V_A , where diffusion from the plasma volume is the only source of the stable products N_2, O_2, NO and NO_2; where the precursor N_2O is continuously renewed mostly by the gas flow input, and where a portion of fresh N_2O is lost, transferred to the plasma volume by diffusion.

Diffusion processes involving the stable species, which are considered to be the only mechanisms of interchange of matter between the two volumes V_P and V_A, are taken into account by means of the corresponding terms included in the differential equations. These terms are formulated by considering a finite difference of the concentrations of each stable species between V_P and V_A at every moment and by estimating the diffusion coefficient D_X of each one of them in a medium where the main species is the precursor N_2O. The diffusion area A and the diffusion length L do not participate in the differential equations separately but as a single parameter A/L, whose value, which should be selected properly, supplies an estimation of the speed or facility of mixing of matter between both volumes.

$O(^1D)$ and N atoms and excited N_2O molecules recombine or de-excite too quickly in the gas phase through homogeneous reactions or quenching, and they do not diffuse appreciably outside the plasma volume V_p; therefore, differential equations for these species corresponding to the volume V_A are not included. The $O(^3P)$ atoms are formed by dissociation of N_2O or by quenching of $O(^1D)$ and do not experience gas phase recombination, but disappear exclusively by adsorption and recombination in the cathode wall. This disappearance processes are very efficient, with a probability $\gamma = 1$, and wall adsorption of $O(^3P)$ atoms is actually limited by diffusion. This fact implies that the $O(^3P)$ concentration may be considered to have a constant value inside the plasma volume and to decrease smoothly out of V_p and towards the neighborhood of the cathode wall until it gets to zero at the stainless steel surface.[29] Nevertheless, in the present model, the cylindrical limits of the plasma volume are very near the cathode walls, and for the sake of simplicity we have just considered $O(^3P)$ atoms confined to the plasma volume, although adsorption and wall recombination

to produce oxygen molecules are taken explicitly into account through reactions W1 and W2 of Table I.

The whole set of differential equations has been numerically solved by means of a fourth order Runge-Kutta method. The solution of these equations yields the time evolution of the concentrations of each species in the volumes V_A and V_P, from the beginning of the experiment until the attainment of the quasi-stationary state of the modulated discharge, which is reached in a time interval of a few seconds and can be compared with the experimental results.

In the same way as in the DC mode of operation, the long term pressure increase experienced by the cell when the present modulated discharge is turned on determines a variation in the output conductances of the experimental system, which were previously calibrated with pure N_2O for different pressures and flow rates, in the absence of discharge. This calibration is incorporated also into the model in order to estimate the residence time, $\tau(t)$, because it influences the removal of the stable species by pumping, especially at low flow rates. In the present model, which takes into account the two different volumes, these pumping terms have been considered twice for each stable species: once in the differential equation corresponding to the volume V_P and the other one in that corresponding to V_A; each one of them with a weight proportional to the respective volume. In the case of atoms and excited molecules, pumping effects can be considered negligible since these species disappear very quickly, and have not been included in the model. The gas flow input of fresh N_2O has been taken also into account separately into two parts, flowing simultaneously to both volumes, each one of them in a quantity proportional to the V_P and V_A values.

4. Results and discussion

Figure 3a shows the temporal variations in the N_2O ground state population produced by the hollow cathode discharge, as derived from the absorbance spectra experimentally observed along the optical path-lenght of the IR beam across the cell. These results were obtained in a 2 mbar, 80 mA, 45 Hz modulated N_2O discharge, at two different gas flow rates, 3 sccm and 108 sccm. In the simple geometrical assumption of the present work, it may be considered that the N_2O population is observed through the V_P and V_A volumes, weighted with their respective optical path-lengths, as displayed in Figure 1.

In Figure 3a, the theoretical results of the present model are given too. In order to compare, the results obtained by applying the former model, in which the stable species are assumed to be homogeneously distributed, are also shown. The large differences between the predictions of the two models are worth noting, both in the amplitude of modulation and in the time evolution of the

calculated signals. The present model, which introduces just two different concentration distributions and incorporates diffusion terms connecting them, leads to an amplitude of oscillation larger by an order of magnitude than that of the former one, hence approaching much better the experimental results as shown in Figure 3a. However, the new amplitudes of oscillation are still smaller than the measured values by a factor between two and five, depending on the flow. The improvement achieved in the prediction of the shape of the modulated signals is apparent in Figure 3b where the time profiles corresponding to the present and to the previous model have been scaled to the measurements. The neglect in the model of N_2O excitation processes (i.e., the assumption $k_{E1} = k_{E2} = 0$) leads to a practical disappearance of the modulation of the N_2O ground state concentration nearly as effective as that obtained by disregarding diffusion effects (i.e., by using the former model),[15] thus indicating that both kinds of processes are essential in order to explain the observed effects in the modulated discharge.

Concerning the diffusion terms of the form $([X]–[X'])D_XA/L$, different values of the ratio A/L between 0.3 and 30 cm have been tried. It has been observed that too small A/L values (too small diffusion area or too large diffusion length) lead to a temporal behavior of the modulated N_2O absorption signal with rise and fall time constants markedly slower than those of the experimental data, and to a slightly higher value of the mean concentration of N_2O in the pseudo-stationary state; whereas too high A/L values (too large diffusion area or too short diffusion length) lead to modulation signals with rise and fall time constants too fast in comparison with the experimental results, as well as to a somewhat lower mean value of the N_2O concentration. In contrast with the very sensitive dependence of the signal time profile on the selected A/L value, it has been observed that the amplitude of modulation is hardly dependent on this parameter, except for its highest values. Finally, a ratio A/L = 10 cm has been selected. This value is consistent with a diffusion length about L ~ 1 - 2 cm and a diffusion area of approximately A ~ 10 - 20 cm^2, which are compatible with the geometry of the plasma volume. The value of L is of the same order as the distance that the stable species involved in the kinetics of the N_2O discharge travel by diffusion during a time interval of ~ 1-2 ms (i.e. during the temporal range of the duration of the transients observed in the present work), and the value of A is intermediate between that of the cathode circular ends (5 cm^2) and that of the plasma surface (35 cm^2), but closer to the first one. Concerning this diffusion area, the logic option at first sight would be to consider a value equal to that limiting the plasma volume; nevertheless one should take into account that diffusion through the curved surface of the plasma cylinder should be significantly limited by the proximity of the cathode wall, which avoids largely

the renewal of fresh N_2O in this direction. Consequently, a diffusion area closer to that of the cathode ends seems more appropriate.

In the preceding papers,[12,13] the plasma volume was thought to be located inside the cathode and to be limited by a cylinder with a radius of 5 mm and a length coincident with that of the cathode, 90 mm, in agreement with the measurements of charge density obtained in ref 12 by a double Langmuir probe; nevertheless, the precise geometrical distribution of the plasma region in those cases was really irrelevant and only its total volume had to be taken into account because, for the unstable species, only the plasma size, and not its shape, was considered in the model and, with regard to the concentrations of the stable species, they were supposed homogeneous throughout the whole cell volume. In the present model, the plasma volume (V_P = 7 cm^3) has been maintained, but a slightly different geometry has been assumed in order to explain better the experimental data. Figure 4 shows the predicted changes in the ground state populations of N_2O as well as the behavior of the other species, estimated separately for each of the two volumes V_P and V_A considered in the model. The results portrayed in this Figure correspond to the slowest and fastest flow studied. It can be seen clearly that the modulation of the N_2O population in the ground state is only noticeable inside the plasma volume, where all the kinetic processes take place, and is negligible elsewhere in the cell; therefore, it is easy to see that a better agreement with the large modulation amplitude of the experimental results would be obtained if a longer optical path-length of the IR beam could be assumed through the plasma region, V_P, and a correspondingly shorter one could be assumed through V_A. So, an increase of the length of the plasma cylinder was assumed, by extending it to the position of the anodes (140 mm), while accordingly decreasing the value of its radius to 4 mm, in order to maintain the same value of V_P. This geometric distribution of the plasma volume is shown schematically in Figure 1. In any case, the differences between the former and the present V_P dimensions are within the instrumental spatial resolution of the double Langmuir probe, which is limited by its finite dimensions, 1 mm in the transversal direction, defined by the distance between the two wires, and 10 mm in the longitudinal direction, equivalent to their lengths. On the other hand, more recent and sensitive measurements made with the Langmuir probe showed that a small charge density (~ 10%) extends also outside the cathode. Actually, the calculated values of Figure 3 correspond to the effective plasma distribution given above (a cylinder 140 mm long and with a radius of 4 mm) and displayed in Figure 1. A further lengthening of the plasma region preserving its volume would increase even further the amplitude of modulation of the signal corresponding to the ground state population of N_2O, and would improve the agreement between the predicted values and the experimental data.

Besides the ground state population of the precursor, Figure 4 shows the concentrations of the stable products of the discharge N_2 and O_2 inside and outside the plasma volume (V_P and V_A), within two periods of the 45 Hz modulated discharge, for the two gas flow rates, 3 and 108 sccm. Their concentrations are remarkably smaller than that of the precursor for the highest flow rate (108 sccm) but increase above the N_2O concentration for 3 sccm. The population of the (001) vibrational level of N_2O is displayed too, but only in the plasma volume where it is assumed to be confined; the concentration of NO and NO_2 in both volumes and of the unstable species in V_P are too small to be shown in a linear scale in Figure 4. As can be seen in the lower panels of this figure, the concentrations of the precursor and of the stable species N_2 and O_2 outside the plasma volume do not undergo any appreciable modulation following the modulation of the discharge at this frequency. This fact justifies the lack of detection of modulated N_2O, N_2 and O_2 signals at 45 Hz when studied by mass spectrometry. On the contrary (upper panels of Figure 4), a modulation is seen in the simulation inside the plasma volume for all of these species, although with time constants much slower than those corresponding to excitation and de-excitation of N_2O. This is in agreement with the slower nature of the dissociation and recombination processes in the N_2O discharge. For the (001) vibrational mode of N_2O, a modulated behavior similar to the ground state of the precursor but with a phase difference of 180º can be noticed.

The slower processes just mentioned begin to be relevant with decreasing discharge frequencies. Modulation of the N_2O, N_2 and O_2 concentrations outside the plasma volume, which begins to be noticeable below ~ 20 Hz and increases in amplitude at lower frequencies, can be detected by mass spectrometric measurements. These results are shown in Figure 5, where the mass spectrometer outputs in mV of N_2O (44 a.m.u.), N_2 (28 a.m.u.) and O_2 (32 a.m.u.) sampled at one end of the discharge cell are drawn at modulation frequencies of 1 Hz (left-bottom panel) and 20 Hz (right-bottom panel) for a 1 mbar, 36 sccm, 100 mA discharge and are compared with the absolute concentration values predicted in the V_A volume by the present theoretical model. The good global agreement between experiment and theory is worth noting. In the upper panels of Figure 5, the theoretical predictions of the time evolution of these major species inside the plasma volume V_P are shown too; their behaviors display larger and more sudden concentration variations than those predicted and observed experimentally in V_A; consequently, this fact confirms once more the existence of diffusion effects, which are not noticeable either in DC discharges, or in typical high frequency (e. g. microwave or radio-frequency) discharges , but can be evinced by a suitable choice of the range of discharge modulation frequencies.

In order to demonstrate further the validity of the present kinetic model, Figure 6 shows the simulation of the ignition and the extinction of the continuous N_2O discharge, which was studied in an earlier work,[13] until the attainment of the respective stationary states, and its comparison with the theoretical predictions of the former model. Only the concentrations of the stable species are shown in this figure for a gas flow rate of 3 sccm with the A/L value of 10 cm previously used, and a very encouraging agreement can be observed to exist between both models. The agreement reached for the unstable species (not shown for clarity of display) is as good as that for the stable ones. When the ratio A/L is very large, the diffusion processes become instantaneous; then the concurrence between the numerical predictions of both models is complete, since conceptually they become the same. If the A/L ratio were diminished markedly under the value used in the present work, slight discrepancies would appear with the experimental results as well as with the predictions of the former model. In that case, fresh N_2O would be renewed much more slowly inside the plasma region and a smaller decrease in N_2O dissociation would be obtained; consequently, lower concentration of the major products N_2 and O_2 would be achieved too, and the fast transient behavior of NO and NO_2 at the ignition of the discharge would be slower.

5. Summary and Conclusions

In this work the time evolution of the ground state N_2O concentration associated with fast transients of a 45 Hz, square wave modulated, hollow cathode discharge of nitrous oxide has been studied, once the slow transients corresponding to the ignition of the modulated discharge have finished. In order to achieve the needed time resolution in the order of a millisecond, the former experimental scheme had to be improved and a step-scan mode of detection for absorption measurements was implemented in the FTIR spectrometer. This is a non-trivial modification and, as far as we know, very few time-resolved absorption measurements with a step-scan FTIR instrument have been reported previously

In contrast to the behavior observed in the N_2O infrared data, which correspond to the whole length of the discharge cell, mass spectrometric measurements, performed at the end of the cell (i.e. outside the plasma volume) have revealed that in order to observe a significant modulation in the concentration of the major species (N_2O, N_2, and O_2), the modulation frequencies have to go well below 20 Hz.

In order to justify the experimental results, an improved kinetic model based on previous works has been used. Within this model, the fast transient behavior of the N_2O ground state population is attributed to the excitation of the vibrational symmetric and asymmetric stretching

modes of this molecule, combined with the assumption of a non uniform distribution of concentrations along the whole cell and with the occurrence of diffusion effects. On the other hand, the modulation of concentration of the major products observed at one end of the cell confirms the inhomogeneous distribution of species and the diffusion effects, independently of vibrational excitation processes. In an attempt to keep the model uncomplicated, the new data have been treated in the simplest way compatible with the observations, namely by dividing the cell volume into two (one for the plasma and the other one for the rest) interconnected by diffusion. These assumptions had not been included in previous studies of N_2O plasmas performed on the stationary state of MW, RF and DC discharges[7,8,12] but they are necessary to explain the present experimental data. With this modifications of the model, the agreement with the continuous and the slow transient results of previous works[12,13] is maintained. The present results, as well as those obtained in ref 13 show the advantages of modulated discharges as compared with continuous ones. The use of different modulation frequencies can provide different time-scales, which can be of great help to elucidate the elementary physico-chemical processes happening inside the plasma.

Further improvements intended to account for larger variations in the population of the N_2O ground state and that could fit better the experimental amplitude of modulation obtained in this work would have to include most surely additional N_2O excitation channels and a more precise knowledge of the geometrical distribution of the various species within the plasma, as well as a refined position dependent treatment of the diffusion effects.

Aknowledgment. The technical advice and support of J. M. Castillo, M. A. Moreno and J. Rodríguez have been most valuable for the achievement of the present experiments. The SEUID of Spain (Projects PB98-0762-C03-02 and PB96-0881) and the Consejería de Educación y Cultura, C.A.M. (Project 07N/0024/1999) are gratefully acknowledged for financial support.

REFERENCES

(1) Grill, A. *Cold Plasma in Materials Fabrication*, IEEE Press: New York, **1993**.

(2) Yamaguchi, T. ; Sakamoto, N. ; Shimozuma, M. ; Yoshino, M. ; Tagashira, H. *J. Appl. Phys.* **1998**, *83*, 554.

(3) Miyama, M.; Yasuda, H. K. *J. Appl. Polym. Sci.* **1998,** *70*, 237.

(4) Bacci, T.; Borchi, E.; Bruzzi, M.; Santoro, M.; Sciortino, *S. Inorg. Mater.* **1998**, *34*, 321.

(5) Hellmich, A.; Jung, T.; Kielhorn, A.; Rissland, *M Surf. Coat. Technol.* **1998**, *98*, 1541

(6) Tabarés, F. L.; Tafalla, D.; de la Cal, E. *Recent Res. Devel. Vacuum Sci. & Tech*. **1999**, *1*, 93.

(7) Cleland, T. A.; Hess D. W. J. Electrochem. Soc. **1989**, 136, 3103.

(8) Kline, L. E.; Partlow, W. D.; Young, R. M.; Mitchell, R. R.; Congedo, T. V.IEEE Transactions on Plasma Science. **1991**, 19, 278.

(9) O'Neil, J. A. *J. Vac. Sci. Technol. A* **1991**, *9*, 669.

(10) Ung, A. Y. M. *Chem. Phys. Lett.* **1975**, *32*, 351.

(11) Piper, L. G.†; Rawlins, W. T. *J. Phys. Chem.* **1986**, *90*, 321.

(12) Arcos, T.; Domingo, C.; Herrero, V. J.; Sanz, M. M.; Shulz, A.; Tanarro, I. J. Phys. Chem. A **1998**, 102, 6282.

(13) Arcos, T.; Domingo, C.; Herrero, V. J.; Sanz, M. M.; Schulz, A.; Tanarro, I. *J. Phys. Chem. A* **2000**, *104*, 3974.

(14) Hayashi, M.; Niwa, A. Proceedings of the 5th Int. Symp. on Gaseous Dielectrics; Christophorou, L. G.; Ed.; 1987.

(15) Arcos, T. Espectroscopía y dinámica de plasmas de N_2O en descargas de cátodo hueco; Ph. D. Thesis, Madrid, 1998.

(16) Arslanbekov, R. R.; Kudryavtsev, Proceedings of the NATO Advanced Research Workshop on Electron Kinetics and Applications of Glow Dischargers, Kortshagen, U.; Tsedin, L. D. Eds, NATO ASI Series Book, Plenum: New York **1998**.

(17) Hartland, G. V.; Xie, W.; Dai, H-L. *Rev. Sci. Instrum.* 1992, *63*, 3261.

(18) Hancock, G.; Heard, D. E. Time-resolved FTIR emission studies of photochemical reactions, in *Advances in Photochemistry,* Vol 18, D. Volman, G. S. Hammond and D. C. Neckers (Eds.), John Wiley and Sons 1993.

(19) Manning, C. J.; Griffiths, P. R. *Appl. Spectrosc.* **1997,** *8*, 1092.

(20) Sloan, J. J.; Kruus, E. J. Time-resolved Fourier Transform Spectroscopy in *Time Resolved Spectroscopy*, Clark, R. J. H.; Hester, R. E., Eds.; John Wiley and Sons: Chichester, 1989; Chapter 5.

(21) Murphy, R. E.; Sakai, H. *Proceedings of the Aspen International Conference on Fourier Spectroscopy*, Vanasse, G. A.; Stain, A. T.; Baker, D. J. Eds., Air Force Cambridge Research Laboratory Special Report No.114, 1970, p.301.

(22) Murphy, R. E.; Cook, F. H.; Sakai, H. *J. Opt. Soc. Am.* **1975**, ***65***, 600.

(23) Uhmann,W.; Becker, K.; Taran, C.; Siebert, F. *Applied Spectrosc.* **1991,** *45*, 390.

(24) Hutson, M. S.; Braiman, M. S. *Appl. Spectrosc.* **1998**, *52*, 974.

(25) Benidar, A.; Guelachvili, P. A.; Martin, P. A. *Chem. Phys. Lett.* **1991**, *177*, 563.

(26) Sloan, J. J.; Neil, W. S.; Roscoe, J.; Kong, F. A. 11th Int. Conf. on Fourier Transform Spectroscopy, Athens, GA. (1997).

(27) Manning, C. J.; Palmer, R. A.; Chao, J. L. *Rev. Sci. Instrum.* **1991** *62*, 1219.

(28) Lambert, J. D. *Vibrational and Rotational Relaxation in Gases,* Clarendon Press: Oxford 1977.

(29) Chantry, P. J. *J. Appl. Phys.* **1987**, *62*, 1141.

(30) Huddleston, R. K.; Weitz, E. *J. Chem. Phys.* **1981**, *74*, 2879.

(31) Atkinson, R.; Baulch, D. L.; Cox, R. A.; Hampson, Jr. R. F.; Kerr, J. A.; Rossi, M. J.; Troe, J. *J. Phys. Chem. Ref. Data* **1999**, *28*, 191.

(32) McEwan, M. J. ; Phillips L. F. *Chemistry of the Atmosphere,* John Wiley and Sons: New York, 1975.

(33) Atkinson, R.; Baulch, D. L.; Cox, R. A.; Hampson, Jr. R. F.; Kerr, M. J.; Troe; J. *J. Phys. Chem. Ref. Data* **1989**, *18*, 881.

(34) Yardley, J. T. *Introduction to Molecular Energy Transfer*, Academic Press: London, 1980.

(35) Hirschfelder, J. O.; Curtiss, C. F.; Bird, R. B. *Molecular Theory of Gases and Liquids*; John Wiley & Sons, 1954.

FIGURES

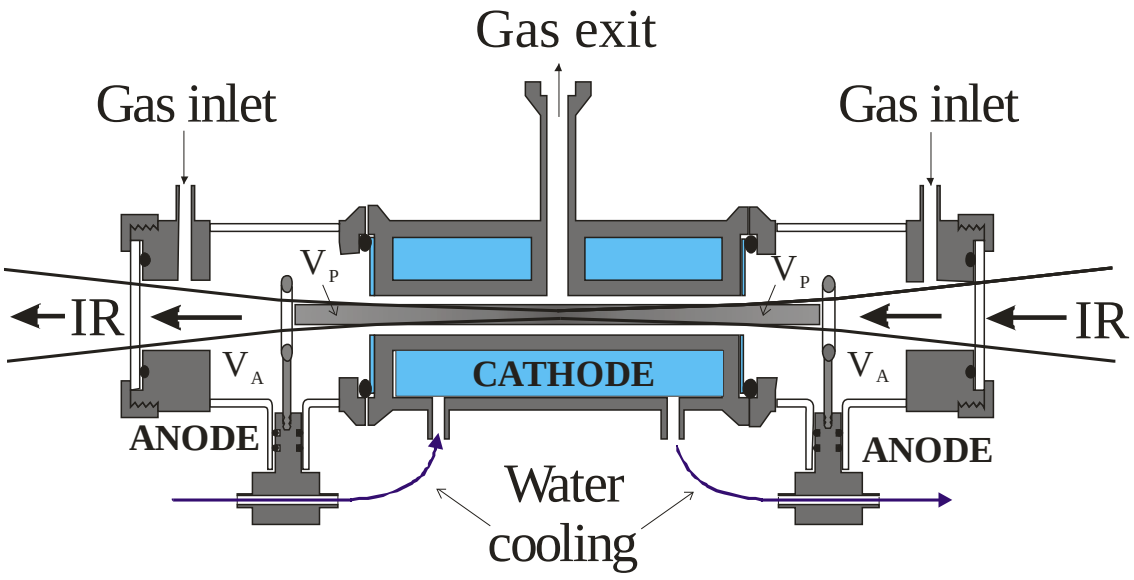

Figure 1 - Scheme of the hollow cathode discharge cell, showing the focusing and the optical path of the IR beam of the FTIR spectrometer across the cell, as well as the location of the plasma region, V_P, and of the rest of the volume without electrical charge, V_A, assumed in the present theoretical model. Mass spectrometry is performed in this cell by replacing one of the IR windows by a flange supporting a central diaphragm with a diameter of 100 μm. Another flange holding the double Langmuir probe can be used in order to measure the charge density and mean electron energy.

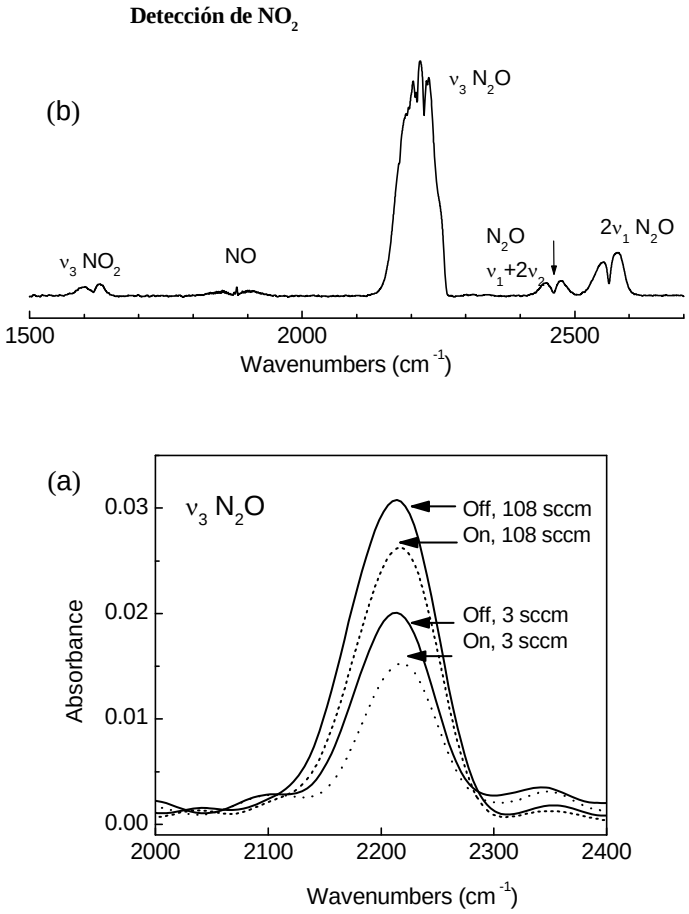

Figure 2 - a) Absorbance spectra of the ν_3 band of N_2O with a spectral resolution of 40 cm^{-1}, at two different moments, with discharge "on" and "off", and at the two different values of N_2O gas flow rates (3 and 108 sccm). Integration of the band was performed between 2100 and 2300 cm^{-1} for obtaining the concentration. b) FTIR rapid-scan spectrum of a DC, 40 mA, 3 sccm, N_2O discharge between 1500 and 2700 cm^{-1} with a spectral resolution of 2 cm^{-1}. Some weak bands of NO and NO_2, as well as the 2 ν_1 and $\nu_1+2\nu_2$ bands of N_2O can be observed.

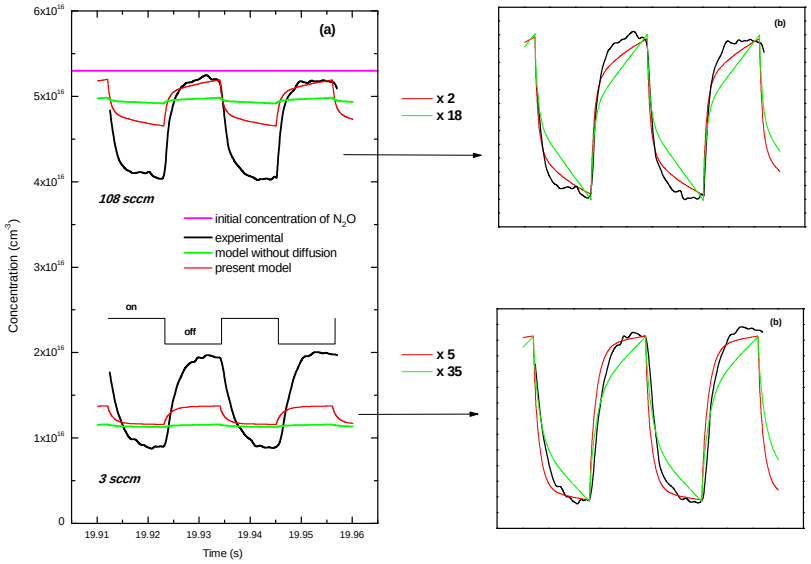

Figure 3 - Temporal evolutions of the N_2O ground state concentration experimentally obtained by FTIR absorption spectroscopy with the hollow cathode discharge cell operating at 45 Hz, 80 mA (maximum current) and 2 mbar, for two gas flow rates, 3 sccm and 108 sccm. The theoretical predictions of the present model, as well as the results of the model of ref 8 are also shown. For a better comparison of the temporal behavior, Fig 2b shows the experimental results and the theoretical predictions with equivalent amplitudes.

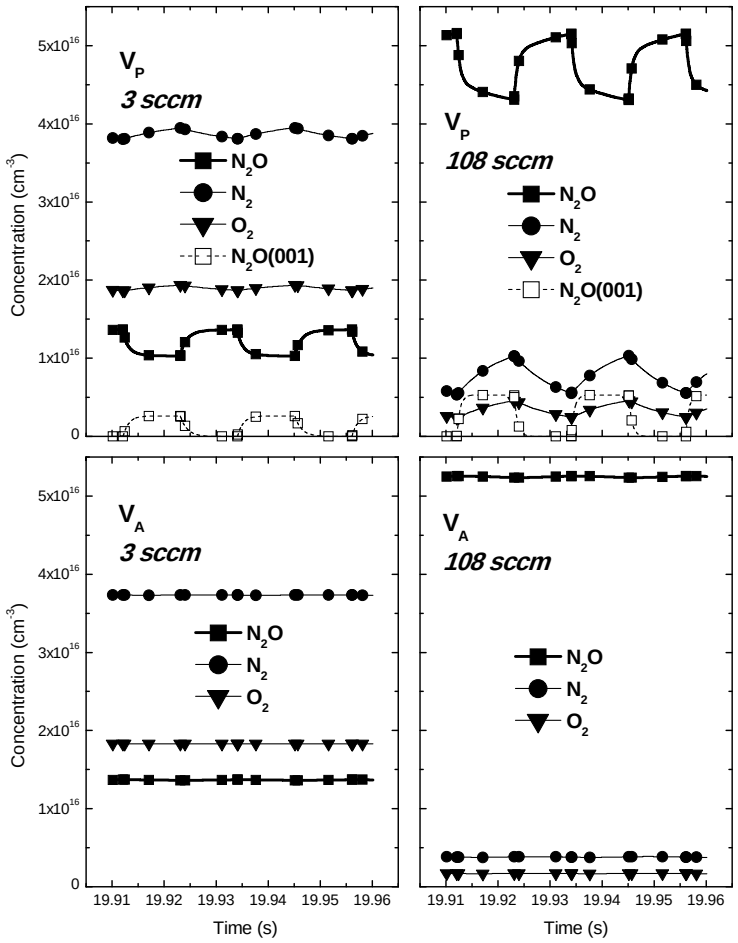

Figure 4 - Theoretical predictions of the time dependent concentrations of the major products of the discharge N_2O, N_2 and O_2 in the two volumes V_P and V_A considered in the present model, with the hollow cathode discharge cell operating at 45 Hz and 2 mbar, for the two gas flow rates, 3 sccm and 108 sccm. The behavior of the (001) vibrational excited level of N_2O in the plasma volume is shown too.

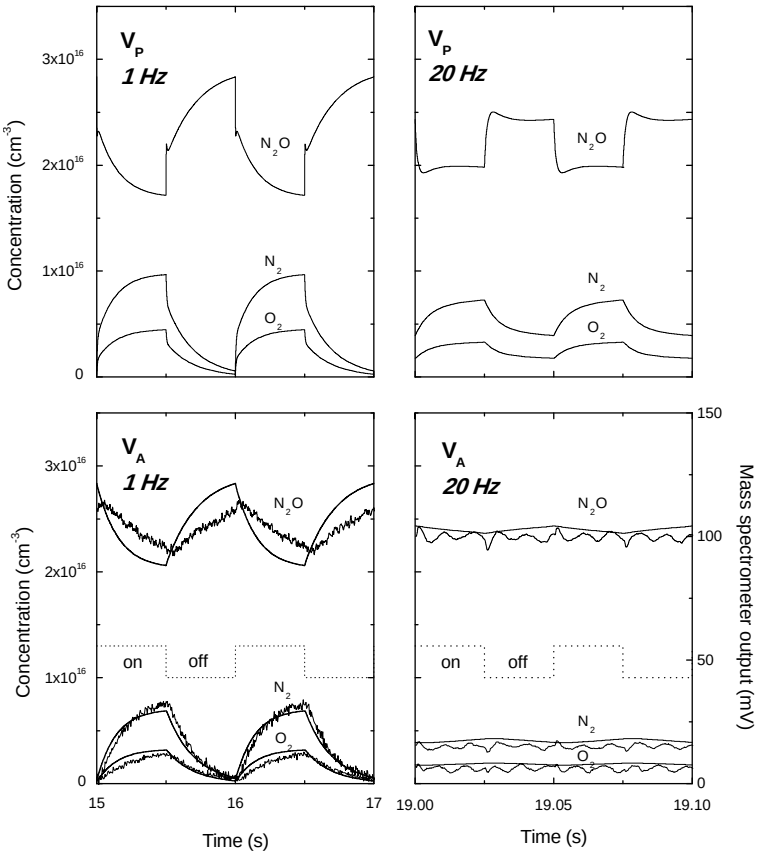

Figure 5 - Mass spectrometer outputs in mV of N_2O (44 a.m.u), N_2 (28 a.m.u) and O_2 (32 a.m.u) sampled at one edge of the discharge cell, drawn at modulation frequencies of 1 Hz (left-bottom panel) and 20 Hz (right-bottom panel) for a 1 mbar, 36 sccm, 100 mA discharge and compared with the absolute concentration values predicted in V_A by the present theoretical model. In the upper panels, the theoretical predictions of the behavior of N_2O, N_2 and O_2 inside the plasma volume, V_P, are shown too.

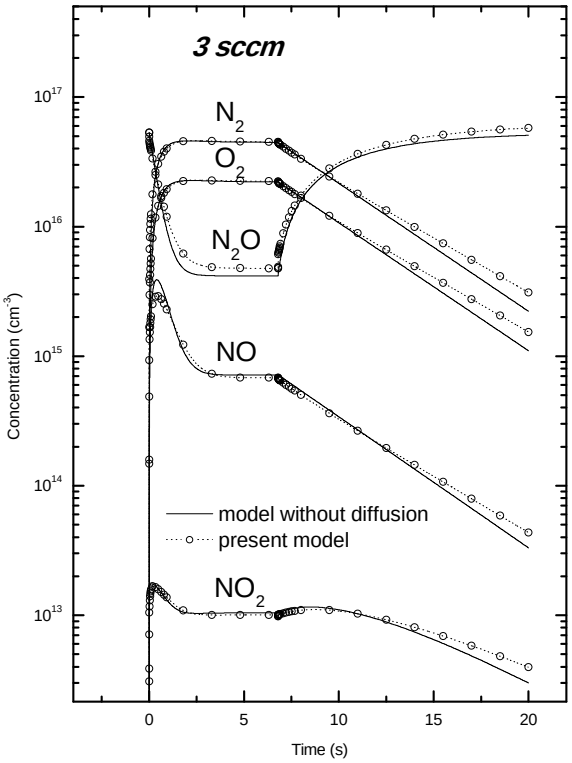

Figure 6 - Simulation of the ignition and the extinction of the continuous N_2O discharge with the present model until the attainment of the respective stationary states and comparison with the theoretical predictions obtained without including diffusion effects.[8]

TABLE I: Reactions included in the kinetics model of the N_2O hollow cathode discharge. Rate coefficients are in units of cm^3 $molecule^{-1}$ s^{-1} for dissociation by electronic impact and bimolecular reactions; cm^6 $molecule^{-2}$ s^{-1} for trimolecular reactions and s^{-1} for heterogeneous reactions. The diffusion coefficients are included as well in units of cm^2s^{-1}.

	REACTION	**Rate constant**	**ref.**
	Dissociation by electronic impact		
D_1	$N_2O + e^- \rightarrow N_2 + O(^3P) + e^-$		
D_1	$N_2O(001) + e^- \rightarrow N_2 + O(^3P) + e^-$	8.0×10^{-10}	***a***
D_1	$N_2O(100) + e^- \rightarrow N_2 + O(^3P) + e^-$		
D_2	$N_2O + e^- \rightarrow N_2 + O(^1D) + e^-$		
D_2	$N_2O(001) + e^- \rightarrow N_2 + O(^1D) + e^-$	$3.7 \times. 10^{-10}$	***a***
D_2	$N_2O(100) + e^- \rightarrow N_2 + O(^1D) + e^-$		
D_3	$N_2O + e^- \rightarrow NO + N + e^-$		
D_3	$N_2O(001) + e^- \rightarrow NO + N + e^-$	1.2×10^{-10}	***a***
D_3	$N_2O(100) + e^- \rightarrow NO + N + e^-$		
D_4	$NO + e^- \rightarrow N + O(^3P)$	8.5×10^{-10}	***a***
D_5	$NO_2 + e^- \rightarrow NO + O(^3P) + e^-$	8.5×10^{-10}	***a***
D_6	$O_2 + e^- \rightarrow 2\ O(^3P) + e^-$	4.8×10^{-11}	***a***
D_7	$O_2 + e^- \rightarrow O(^3P) + O(^1D) + e^-$	7.2×10^{-11}	***a***
	Electronic impact excitation		
E_1	$N_2O + e^- \rightarrow N_2O(001) + e^-$	1.4×10^{-8}	***b***
E_2	$N_2O + e^- \rightarrow N_2O(100) + e^-$	1.4×10^{-8}	***b***
	Quenching of excited states		
Q_1	$N_2O(001) + N_2O \rightarrow 2\ N_2O$	2.44×10^{-14}	10
Q_2	$N_2O(100) + N_2O \rightarrow 2\ N_2O$	5.26×10^{-13}	30
Q_3	$O(^1D) + N_2 \rightarrow O(^3P) + N_2$	2.6×10^{-11}	31
Q_4	$O(^1D) + NO \rightarrow O(^3P) + NO$	1.5×10^{-10}	32
	Homogeneous reactions		
G_1	$N_2O + O(^1D) \rightarrow 2\ NO$		
G_1	$N_2O(001) + O(^1D) \rightarrow 2\ NO$	7.2×10^{-11}	31
G_1	$N_2O(100) + O(^1D) \rightarrow 2\ NO$		
G_2	$N_2O + O(^1D) \rightarrow N_2 + O_2$		
G_2	$N_2O(001) + O(^1D) \rightarrow N_2 + O_2$	4.4×10^{-11}	31
G_2	$N_2O(100) + O(^1D) \rightarrow N_2 + O_2$		
G_3	$N_2O(001) + O(^1D) \rightarrow NO_2 + N$	1.0×10^{-10}	***a***
G_4	$NO + O(^3P) + M \rightarrow NO_2 + M$	10^{-31}	31
G_5	$NO_2 + O(^1D) \rightarrow NO + O_2$	3.0×10^{-10}	***a***
G_6	$NO_2 + O(^3P) \rightarrow NO + O_2$	9.7×10^{-12}	31
G_7	$NO + N \rightarrow N_2 + O(^3P)$	3.0×10^{-11}	33
G_8	$NO + O(^1D) \rightarrow O_2 + N$	8.5×10^{-11}	33

	Heterogeneous Reactions		
W_1	$O(^1D) + wall \rightarrow O(^3P)$	2200	***c***
W_2	$O(^3P) + wall \rightarrow O(S)$	2200	***c***
W_3	$O(^3P) + O(S) \rightarrow O_2$	180	7
W_4	$N + wall \rightarrow (1/2)\, N_2$	16.1	***c***
W_5	$N_2O(001) + wall \rightarrow N_2O$	222	***c***
W_6	$N_2O(100) + wall \rightarrow N_2O$	222	***c***
W_7	$NO + O(S) \rightarrow NO_2$	2.75×10^{-3}	***a***
	Radiative Deexcitation		
R_1	$N_2O(001) \rightarrow N_2O$ ($\tau_1 \sim 4$ ms)	258	15
R_2	$N_2O(100) \rightarrow N_2O$ ($\tau_2 \sim 83$ ms)	12	34
	Diffusion Coefficients		
D_{N2O}		71.5	***d***
D_{O2}		84.0	***d***
D_{N2}		79.0	***d***
D_{NO}		84.0	***d***
D_{NO2}		71.0	***d***

(a) Estimated in this work.
(b) Calculated from ref. 14
(c) Calculated in our cell geometry assuming γ=1 (see text).
(d) The diffusion coefficients have been estimated by using the approximation of rigid spheres[35] for a temperature of 300 K and a pressure of 2 mbar. The diffusion coefficients have been estimated for all gases in N_2O, the main species in the discharge. Molecular diameters have been taken from reference 30. The value of the molecular diameter for NO_2 has been assumed to be the same as that for N_2O.

TABLE II . Set of coupled differential equations obtained from the reactions included in Table I. ϕ_{N2O} is the flow rate of N_2O into the reactor in molecules s^{-1}, V_R is the reactor volume (cm^3) , V_P the plasma volume (cm^3) , V_A, the volume of the whole reactor minus the plasma volume (cm^3), S_C the cathode surface (cm^2), V_C the cathode volume (cm^3) and τ the reactor residence time (s). D_X are the diffusion coefficients for the different species. A is the transversal area where the diffusion takes place (cm^2) and L is the diffusion length. The first ten equations account for the evolution of the concentrations of the different species inside de plasma volume. The eleventh one accounts for atomic oxygen adsorbed in the cathode wall, and the last five ones indicate those of the different species in the volume V_A without plasma.

$$V_P \frac{d[N_2O]_P}{dt} = \Phi_{N_2O}\frac{V_P}{V_R} - (k_{D1}+k_{D2}+k_{D3}+k_{E1}+k_{E2})[N_2O]_P[e^-]V_p + k_{Q1}[N_2O]_P[N_2O(001)]V_P - (k_{G1}+k_{G2})[N_2O]_P[O(^1D)]V_P + k_{Q2}[N_2O]_P[N_2O(100)]V_P + k_{W5}[N_2O(001)]V_P + k_{W6}[N_2O(100)]V_P + [N_2O(001)]\frac{V_P}{\tau_1} + [N_2O(100)]\frac{V_P}{\tau_2} - [N_2O]_P\frac{V_P}{\tau} - D_{N_2O}\frac{A}{L}\{[N_2O]_P - [N_2O]_A\}$$

$$V_P \frac{d[NO]_P}{dt} = k_{D3}[e^-]V_P\{[N_2O]_P + [N_2O(001)] + [N_2O(100)]\} + 2k_{G1}[O(^1D)]V_P\{[N_2O]_P + [N_2O(001)] + [N_2O(100)]\} - k_{G7}[NO]_P[N]V_P - k_{G4}[NO]_P[O(^3P)][M]V_P - k_{D4}[NO]_P[e^-]V_P + k_{D5}[NO_2]_P[e^-]V_P + k_{G6}[NO_2]_P[O(^3P)]V_P - k_{W7}[NO]_P[O(S)]V_C S_C - k_{G8}[NO]_P[O(^1D)]V_P + k_{G5}[NO_2]_P[O(^1D)]V_P - \frac{V_P}{\tau}[NO]_P - D_{NO}\frac{A}{L}\{[NO]_P - [NO]_A\}$$

$$V_P \frac{d[N_2]_P}{dt} = (k_{D1}+k_{D2})[e^-]V_P\{[N_2O]_P + [N_2O(001)] + [N_2O(100)]\} + k_{G2}[O(^1D)]V_P\{[N_2O]_P + [N_2O(001)] + [N_2O(100)]\} + k_{G7}[NO]_P[N]V_P + \frac{1}{2}k_{W4}[N]V_P - \frac{V_P}{\tau}[N_2]_P - D_{N_2}\frac{A}{L}\{[N_2]_P - [N_2]_A\}$$

$$V_P \frac{d[O_2]_P}{dt} = k_{G2}[O(^1D)]V_P\{[N_2O]_P + [N_2O(001)] + [N_2O(100)]\} + k_{W3}[O(^3P)][O(S)]V_P + k_{G5}[O(^1D)][NO_2]V_P + k_{G6}[O(^3P)][NO_2]V_P - (k_{D6}+k_{D7})[O_2][e^-]V_P + k_{G8}[O(^1D)][NO]V_P S_C - [O_2]_P\frac{V_P}{\tau} - D_{O_2}\frac{A}{L}\{[O_2]_P - [O_2]_A\}$$

$$V_P \frac{d[NO_2]_P}{dt} = -k_{D5}[NO_2]_P[e^-]V_P + k_{G3}[O(^1D)][N_2O(001)]V_P + k_{G4}[NO]_P[O(^3P)][M]V_P - k_{G5}[O(^1D)][NO_2]_P V_P - k_{G6}[O(^3P)][NO_2]_P V_P + k_{W7}[NO]_P[O(S)]V_C S_C - [NO_2]_P\frac{V_P}{\tau} - D_{NO_2}\frac{A}{L}\{[NO_2]_P - [NO_2]_A\}$$

$$V_P \frac{d[O(^1D)]}{dt} = k_{D2}\{[N_2O]_P + [N_2O(001)] + [N_2O(100)]\}[e^-]V_P + k_{D7}[e^-][O_2]_P V_P - k_{Q3}[N_2]_P[O(^1D)]V_P$$
$$- (k_{Q4} + k_{G8})[NO]_P[O(^1D)]V_P - (k_{G1} + k_{G2})[O(^1D)]\{[N_2O]_P + [N_2O(001)] + [N_2O(100)]\}V_P$$
$$- k_{G3}[N_2O(001)][O(^1D)]V_P - k_{G5}[NO_2]_P[O(^1D)]V_P - k_{W1}[O(^1D)]V_P$$

$$V_P \frac{d[O(^3P)]}{dt} = k_{D1}\{[N_2O] + [N_2O(001)] + [N_2O(100)]\}[e^-]V_P + k_{D4}[NO]_P[e^-]V_P + k_{D5}[NO_2]_P[e^-]V_P + (2k_{D6} + k_{D7})[O_2]_P[e^-]V_P$$
$$+ k_{Q3}[O(^1D)][N_2]_P V_P + k_{Q4}[O(^1D)][NO]_P V_P - k_{G4}[O(^3P)][NO]_P[M]V_P - k_{G6}[O(^3P)][NO_2]_P V_P - k_{G7}[NO]_P[N]V_P$$
$$+ k_{W1}[O(^1D)]V_P - k_{W2}[O(^3P)]V_P - k_{W3}[O(^3P)][O(S)]V_P S_C$$

$$V_P \frac{d[N_2O(001)]}{dt} = - (k_{D1} + k_{D2} + k_{D3})[N_2O(001)][e^-]V_P + k_{E1}[N_2O]_P[e^-]V_P - (k_{G1} + k_{G2} + k_{G3})[N_2O(001)][O(^1D)]V_P$$
$$- k_{Q1}[N_2O(001)][N_2O]_P V_P - k_{W5}[N_2O(001)]V_P - [N_2O(001)]\frac{V_P}{\tau_1}$$

$$V_P \frac{d[N_2O(100)]}{dt} = - (k_{D1} + k_{D2} + k_{D3})[N_2O(100)][e^-]V_P + k_{E2}[N_2O]_P[e^-]V_P - k_{Q2}[N_2O(100)][N_2O]_P V_P$$
$$- (k_{G1} + k_{G2})[N_2O(100)][O(^1D)]V_P - k_{W6}[N_2O(100)]V_P - [N_2O(100)]\frac{V_P}{\tau_2}$$

$$V_P \frac{d[N]}{dt} = k_{D3}\{[N_2O]_P + [N_2O(001)] + [N_2O(100)]\}[e^-]V_P + k_{D4}[NO]_P[e^-]V_P$$
$$+ k_{G3}[N_2O(001)][O(^1D)]V_P - k_{G7}[NO]_P[N]V_P + k_{G8}[NO]_P[O(^1D)]V_P - k_{W4}[N]V_P$$

$$S_C \frac{d[O(S)]}{dt} = k_{W2}[O(^3P)]V_P - k_{W3}[O(^3P)][O(S)]V_P S_C - k_{W7}[NO]_P[O(S)]V_C S_C$$

$$V_A \frac{d[N_2O]_A}{dt} = \Phi_{N_2O}\frac{V_A}{V_R} - [N_2O]_A\frac{V_A}{\tau} - D_{N_2O}\frac{A}{L}\{[N_2O]_A - [N_2O]_P\}$$

$$V_A \frac{d[NO]_A}{dt} = -\frac{V_A}{\tau}[NO]_A - D_{NO}\frac{A}{L}\{[NO]_A - [NO]_P\}$$

$$V_A \frac{d[N_2]_A}{dt} = -\frac{V_A}{\tau}[N_2]_A - D_{N_2}\frac{A}{L}\{[N_2]_A - [N_2]_P\}$$

$$V_A \frac{d[O_2]_A}{dt} = -\frac{V_A}{\tau}[O_2]_A - D_{O_2}\frac{A}{L}\{[O_2]_A - [O_2]_P\}$$

$$V_A \frac{d[NO_2]_A}{dt} = \quad -\frac{V_A}{\tau}[NO_2]_A - D_{NO_2}\frac{A}{L}\{[NO_2]_A - [NO_2]_P\}$$